

NUMERICAL INVESTIGATION OF LIQUID FILM INSTABILITIES AND EVAPORATION IN CONFINED OSCILLATING SLUG-PLUG FLOWS

MANOLIA ANDREDAKI, ANASTASIOS GEORGOULAS, NICOLAS MICHE & MARCO MARENGO
Advanced Engineering Centre, School of Computing Engineering and Mathematics, University of Brighton, UK

ABSTRACT

An enhanced volume of fluid (VOF)-based numerical simulation framework that accounts for conjugate heat transfer between solid and two-phase flow regions and phase-change due to boiling/condensation, is utilised in order to investigate the effect of flow oscillation amplitude and frequency on the liquid film evaporation and instability formation in slug-plug flows within heated channels, in saturated flow boiling conditions. Various series of parametric numerical simulations are performed, for different values of flow oscillation amplitude and frequency for a variety of working fluids. For one of the working fluids two different channel diameters are also tested. The oscillations in each case are induced by applying an oscillating pressure boundary condition at the inlet of the channel, keeping the pressure constant at the outlet, after an initial period of constant pressure drop between the inlet and the outlet. Capillary ridges that are initiated at the liquid film, in the vicinity of the leading edge of the considered vapour slugs, are identified as a result of the imposed oscillations, which are translated in the form of capillary waves towards the rear end of the bubbles. It is shown that the formation frequency as well as the geometric characteristics of the generated ridges, are directly related to the corresponding frequency and amplitude of the induced flow oscillations. Furthermore, it is shown that in the initial stages of the bubble fate after the application of the oscillations liquid film evaporation is enhanced with the increase of the oscillation amplitude while it degrades as the frequency of the oscillation becomes higher. However, for large oscillation amplitudes and channel diameters, liquid jets penetrate into the elongated bubbles leading in a lot of cases to bubble break-up.

Keywords: volume of fluid, conjugate heat transfer, oscillating vapour slug, micro-channel.

1 INTRODUCTION

The demand for increasingly higher performances of electronic equipment, has pushed in the development of a new generation of heat transfer systems based on the local phase-change of a working fluid. Efficient thermal control, of densely packed electronic components, has become of crucial importance. Flow boiling within micro-channels, constitute one of the most promising cooling technologies to dissipate high heat fluxes from micro-scale electronic components. Two-phase cooling devices utilising evaporators consisting of micro-channels that are in direct contact with a micro-chip, can remove heat fluxes up to 300 W/cm^2 [1]. However, the flow complexity in cases of multi-microchannel two-phase flow evaporators, can lead to high-amplitude and high-frequency temperature and pressure oscillations [2]. Such oscillations, in the slug flow regime, may generate significant instabilities in the liquid film that surrounds the elongated vapour slugs. Such flow oscillations and instabilities are also present in the case of oscillating, closed loop, two-phase cooling devices, such as Pulsating Heat Pipes that might consist of micro- (e.g. [3]) or mini-channels (e.g. [4]).

In the present paper, an enhanced volume of fluid (VOF) based numerical simulation framework that accounts for conjugate heat transfer between a solid region and a two-phase flow region with phase-change due to evaporation and/or condensation, is applied in order to investigate the effect of global flow oscillation frequency and amplitude on the liquid film evaporation and in the liquid film instability generation, in the case of confined isolated, elongated vapour slugs, in saturated flow boiling conditions.



The utilised, enhanced, VOF-based numerical model, has been extensively validated in the past (by the same research group as the authors of the present work) against existing analytical solutions and experimental data on adiabatic and diabatic bubble and droplet dynamics [8], [10]–[12]. Some of these validation results are reproduced in Fig. 1. As it can be observed, the proposed VOF-based numerical modelling framework, accurately predicts adiabatic and diabatic bubble and droplet dynamics as well as conjugate heat transfer between solid and fluid domains. Therefore, since all underpinned mechanisms have been validated in the past (interfacial dynamics, phase-change, conjugate heat transfer) it can safely be used for the purposes of the present investigation.

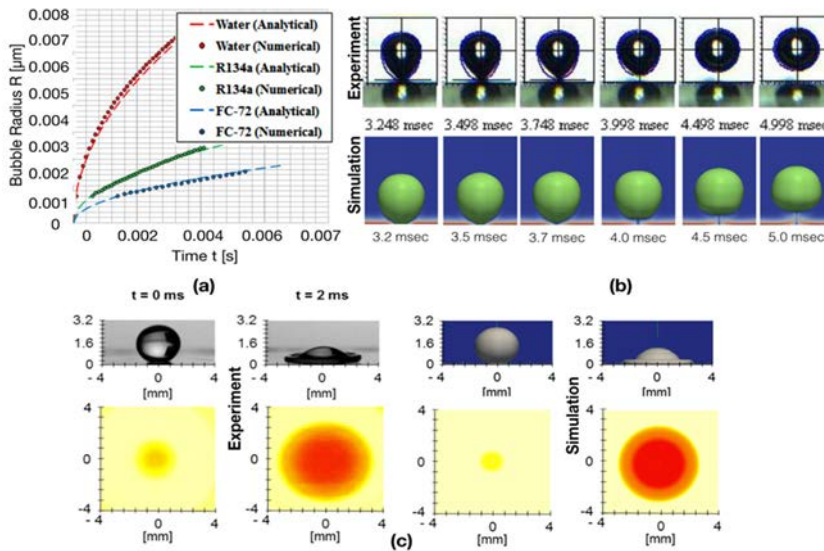


Figure 1: (a) Comparison between numerical simulation and analytical solution results for a bubble evaporating in a superheated domain [10]; (b) Numerical simulation results and experimental results in pool boiling [10]; and (c) Conjugate heat transfer numerical simulation results and experimental measurements on droplet impact cooling [11].

2 INVESTIGATION METHODOLOGY

2.1 Numerical method

2.1.1 Governing equations

In this section, the governing equations for mass, momentum, energy, and volume fraction are presented. It should be mentioned that liquid and vapour phases are both treated as incompressible, Newtonian fluids. The mass conservation equation is given as:

$$\nabla \cdot (\rho \vec{U}) = \dot{\rho}, \quad (1)$$

where \vec{U} is the fluid velocity and ρ is the bulk density. The source term on the right-hand side accounts for the phase change. The conservation of momentum is given by the following equation:

$$\frac{\partial}{\partial t}(\rho \vec{U}) + \nabla \cdot (\rho \vec{U} \vec{U}) - \nabla \cdot \left\{ \mu \left[\nabla \vec{U} + (\nabla \vec{U})^T \right] \right\} = -\nabla p + \vec{f}_{ST} + \vec{f}_g, \quad (2)$$

where p is the pressure and μ is the bulk dynamic viscosity. The momentum source terms on the right-hand side of the equation account for the effects of surface tension and gravity, respectively. The surface tension term is modelled according to the classical approach of Brackbill et al. [5]. The conservation of energy balance is given by the following equation:

$$\frac{\partial}{\partial t}(\rho c_p T) + \nabla \cdot (\vec{U} \rho c_p T) - \nabla \cdot (\lambda \nabla T) = \dot{h}, \quad (3)$$

where c_p is the bulk heat capacity, T the temperature field, and λ is the bulk thermal conductivity. The source term on the right-hand side of the equation represents the contribution of the enthalpy of evaporation/condensation or else the cooling/heating associated with the latent heat of the phase-change. The volume fraction α is advected by the flow field by the following equation:

$$\frac{\partial \alpha}{\partial t} + \nabla \cdot (\alpha \vec{U}) - \nabla \cdot (\alpha(1-\alpha)U_r) = \frac{\dot{\rho}}{\rho} \alpha. \quad (4)$$

Interface sharpening is very important in simulating two-phase flows of two immiscible fluids. In OpenFOAM the sharpening of the interface is achieved artificially by introducing the extra compression term $\nabla \cdot (\alpha(1-\alpha)U_r)$ in eqn (4). U_r is an artificial compression velocity. The divergence of the compression velocity U_r , ensures the conservation of the volume fraction α , while the term $\alpha(1-\alpha)$ limits this artificial compression approach only in the vicinity of the interface, where $0 < \alpha < 1$ [6]. The level of compression depends on the value of C_γ [6], [7]. For the simulations of the present investigation, initial, trial simulations indicated that a value of $C_\gamma = 1$ should be used, in order to maintain a quite sharp interface without at the same time having unphysical results. The source term on the right-hand side of the eqn (4) is needed because, due to the local mass source terms, the velocity field is not free of divergence. Finally, the bulk fluid properties γ are computed as the averages over the liquid (γ_l) and vapour (γ_v) phases, weighted with the volume fraction α . The VOF-based solver that is used in the present investigation has been modified accordingly in order to account for an adequate level of spurious currents suppression. More details on the proposed development and validation as well as on the proposed improved VOF method can be found in the paper by Georgoulas et al. [8].

The conservation of energy equation in the solid domains is defined as:

$$\frac{\partial}{\partial t}(\rho_s c_{ps} T) = \nabla \cdot (\lambda_s \nabla T). \quad (5)$$

The coupling at the interface between the solid region and fluid region is achieved iteratively through the following conditions:

$$T_f = T_s, \quad (6)$$

$$\lambda_f \frac{\partial T_f}{\partial n} = \lambda_s \frac{\partial T_s}{\partial n}. \quad (7)$$

2.1.2 Phase change model

The utilized phase change model that was implemented in the improved OpenFOAM VOF solver that is used in the present investigation, will be described briefly in this section. In the case of evaporation, the evaporating mass flux at the liquid–vapour interface j_{evap} is calculated from the following equation:



$$j_{\text{evap}} = \frac{T_{\text{int}} - T_{\text{sat}}}{R_{\text{int}} h_{\text{lv}}}, \quad (8)$$

where T_{int} is the temperature of the interface, T_{sat} is the saturation temperature, R_{int} is the interfacial heat resistance and h_{lv} is the latent heat of evaporation at the saturation temperature. The amount of liquid that evaporates is calculated locally and the resulting source term field is smeared over a few cells in order to avoid numerical instabilities. The evaporating mass is taken away on the liquid side of the interface and reappears on the vapour side, following the process originally suggested in the work of Hardt and Wondra [9]. Further details on the proposed development can be found in the work of Georgoulas et al. [10].

3 APPLICATION OF NUMERICAL METHOD

3.1 Set-up of numerical simulations

In the current section of the present work the previously described, VOF-based, numerical simulation framework is further applied for the conduction of parametric numerical simulations, aiming to identify and quantify the effect of global flow oscillation frequency and amplitude on the liquid film evaporation and instability formation, around isolated, elongated vapour slugs, within a heated micro-channel, in saturated flow boiling conditions. In more detail, various series of parametric numerical experiments are conducted, applying a constant heat flux value of $\dot{q} = 5,000 \text{ W/m}^2$ in the heated section of the two in total considered circular micro-channels with external and internal diameter values of $D_o = 0.69$ and 1.19 mm and $D_i = 0.5$ and 1.00 mm, respectively. In each series of parametric numerical simulations, the imposed global flow oscillation amplitude and frequency are varied. The flow oscillations are generated inducing an oscillating pressure boundary condition at the inlet of the channel while keeping the pressure constant at the outlet. The same values of oscillation amplitude and frequency are tested for four different working fluids: R245fa, FC72, ethanol and water for the $D_i = 0.5 \text{ mm}$ channel (Series A, C, D and E in Table 1) while R245fa only is tested for the $D_i = 1.0 \text{ mm}$ channel (Series B in Table 1). Each simulation is conducted in three stages. At the first stage a single-phase simulation is run with only liquid flowing into the channel, applying a constant pressure drop of $\Delta P = 500$ Pa. In the second stage, after the single-phase flow has reached a quasi-steady state and the hydrodynamic and thermal boundary layers have been developed ($t = 0.2$ s), an elongated vapour slug is patched upstream of the heated section of the channel at a certain distance from the channel inlet, having an initial length of $3x D_i$ and an initial liquid film thickness of $h_{\text{film}(\text{init})} = 20$ μm . This initial vapor slug is then left to be carried away downstream by the previously developed liquid flow, towards the heated section of the circular micro-channel. At the third and final stage, after approximately 0.02 s (depending on the working fluid and diameter) that the vapour slug front has reached approximately the middle of the channel in each case (ensuring that it is almost completely contained within the heated region of the channel), an oscillating relative pressure boundary condition is imposed at the inlet of the channel, keeping the relative pressure at the outlet constant at 0 Pa. The resulting pressure value for the inlet with respect to time, can be described by the following equation

$$P(t) = (1 + \alpha \sin(\pi f t)) P_{\text{ref}} + P_0, \quad (9)$$

where α and f are the amplitude and frequency of the oscillation, while P_0 and P_{ref} are the initial pressure and a reference pressure, respectively. It should be mentioned that for all the simulations presented here, the reference pressure is taken as unity and the initial pressure as

zero. For each channel, an axisymmetric computational domain is constructed with the axis of symmetry coinciding with the central/longitudinal axis of the considered circular micro-channels. The computational domain, mesh and the applied boundary conditions are illustrated in Fig. 2, for each of the considered channel diameters.

Table 1: Inlet pressure oscillation characteristics, working fluids and internal channel diameters for the considered cases.

Case	a (Pa)	f (Hz)	Fluid	D _i (mm)	Case	a (Pa)	f (Hz)	Fluid	D _i (mm)
A1	100,000	500	R245fa	0.5	D1	100,000	500	Ethanol	0.5
A2	100,000	750	R245fa	0.5	D2	100,000	750	Ethanol	0.5
A3	100,000	1000	R245fa	0.5	D3	100,000	1000	Ethanol	0.5
A4	50,000	500	R245fa	0.5	D4	50,000	500	Ethanol	0.5
A5	75,000	500	R245fa	0.5	D5	75,000	500	Ethanol	0.5
A6	200,000	500	R245fa	0.5	D6	200,000	500	Ethanol	0.5
A7	300,000	500	R245fa	0.5	D7	300,000	500	Ethanol	0.5
B1	100,000	500	R245fa	1.0	E1	100,000	500	Water	0.5
B2	100,000	750	R245fa	1.0	E2	100,000	750	Water	0.5
B3	100,000	1000	R245fa	1.0	E3	100,000	1000	Water	0.5
B4	50,000	500	R245fa	1.0	E4	50,000	500	Water	0.5
B5	75,000	500	R245fa	1.0	E5	75,000	500	Water	0.5
B6	200,000	500	R245fa	1.0	E6	200,000	500	Water	0.5
B7	300,000	500	R245fa	1.0	E7	300,000	500	Water	0.5
C1	100,000	500	FC72	0.5	–	–	–	–	–
C2	100,000	750	FC72	0.5	–	–	–	–	–
C3	100,000	1000	FC72	0.5	–	–	–	–	–
C4	50,000	500	FC72	0.5	–	–	–	–	–
C5	75,000	500	FC72	0.5	–	–	–	–	–
C6	200,000	500	FC72	0.5	–	–	–	–	–
C7	300,000	500	FC72	0.5	–	–	–	–	–

The computational domain consists of a solid and a fluid region that are coupled at their interface. The fluid and solid domains consist of a total number of 143,750 and 115,000 computational cells for the 0.5 mm internal diameter channel and 287,500 and 115,000 computational cells for the 1.0 mm internal diameter channel, respectively. The mesh density in each case was selected after an appropriate mesh independency study. A structured mesh, consisting of hexahedral and prismatic elements is used, with a grid clustering towards the coupling interface between the solid and fluid regions. The overall computation domain constitutes a 5° wedge of the circular micro-channel under consideration in each of the two cases, since this is the way that 2D axisymmetric simulations are conducted in OpenFOAM, the open-source CFD platform that is utilized for the overall computations. Table 1 summarizes the imposed oscillation characteristics, the working fluid and the channel diameter for each of the examined cases, in the present numerical investigation. The initial state of the bubble just before the application of the oscillation for each series of parametric numerical simulations is depicted in Fig. 3.

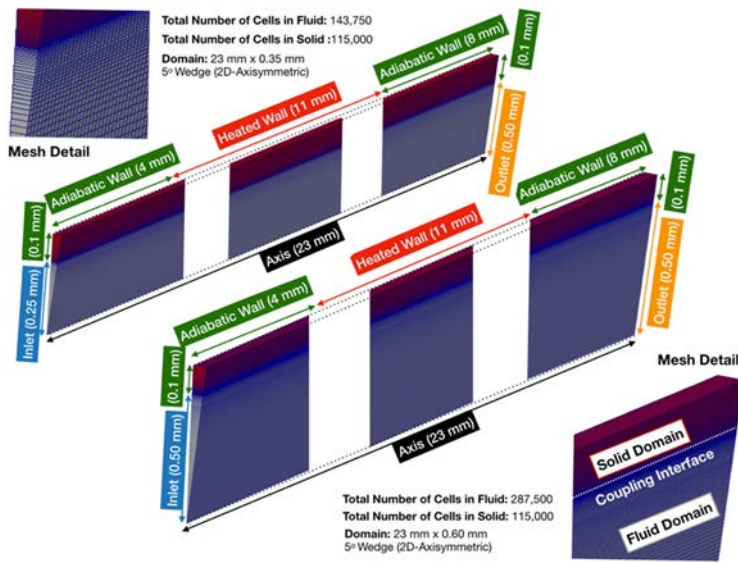


Figure 2: Geometry, Mesh and Boundary conditions, for each of the considered microchannels ($D_i = 0.5$ in the top-left part and $D_i = 1.0$ mm in the bottom-right part of the figure).

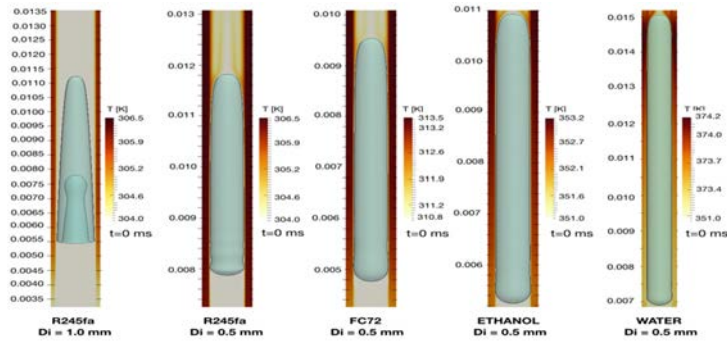


Figure 3: Initial state for all series of parametric numerical simulation (Series A, B, C, D and E), before the application of the fluctuating pressure at the inlet boundary.

3.2 Effect of flow oscillation frequency

The spatial and temporal evolution of the considered vapour slugs in the case of R245fa, under different pressure oscillation frequencies at the inlet of the considered micro-channel, are depicted in Figs 4 and 5 for the $D_i = 0.5$ mm and $D_i = 1.0$ mm channels respectively. Fig. 4 depicts the numerical simulation results for cases A1–A3, while Fig. 5 illustrates the corresponding results for cases B1–B3. In more detail, in both cases the amplitude of the pressure oscillation is kept constant to 100 kPa and the frequency is increased progressively taking the values of 500, 750 and 1000 Hz. As it can be observed, the imposed flow

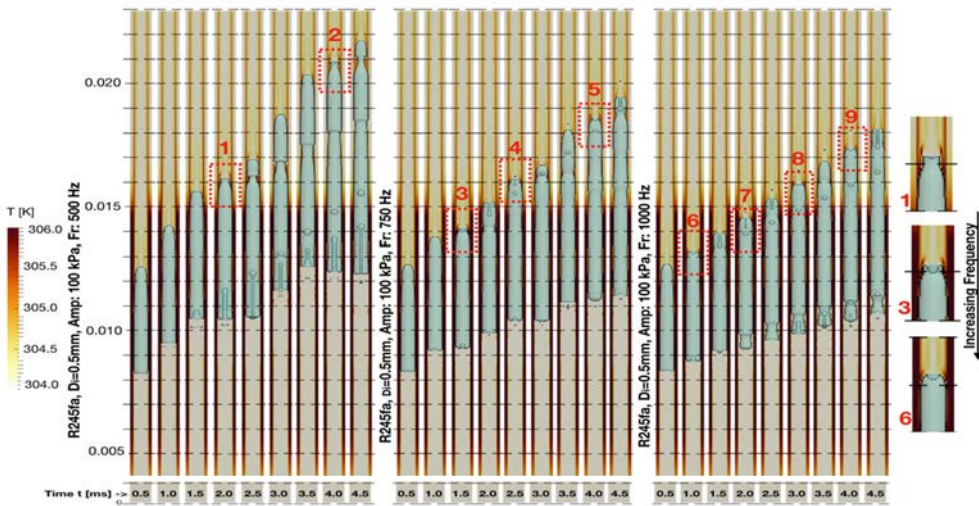


Figure 4: Spatial and temporal evolution of the considered vapour slugs in the case of R245fa, under different pressure oscillation frequencies at the inlet of the considered micro-channel ($D_i = 0.5$ mm). Cases A1 (left), A2 (middle) and A3 (right), from Table 1. The red numbered squares mark the initiation of capillary ridges. A zoomed version of the first instance in each case is also provided.

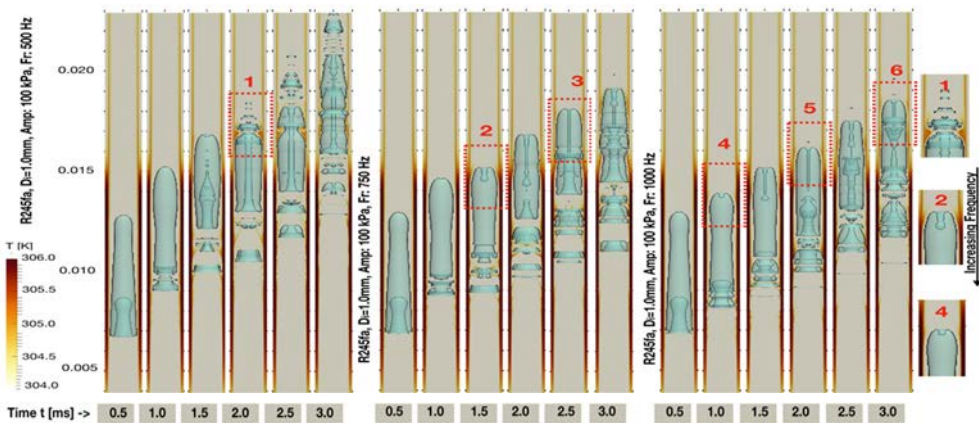


Figure 5: Spatial and temporal evolution of the considered vapour slugs in the case of R245fa, under different pressure oscillation frequencies at the inlet of the considered micro-channel ($D_i = 1.0$ mm). Cases B1 (left), B2 (middle) and A3 (right), from Table 1. The red numbered squares mark the initiation of capillary ridges. A zoomed version of the first instance in each case is also provided.

oscillations are responsible for the periodic generation of a capillary ridges in the vicinity of the leading edge of the evaporating vapour slug. These capillary ridges, after their formation (see for example the numbered red dotted squares in Figs 4 and 5) are then traveling downstream towards the trailing edge of the bubble, gradually attenuating (reducing their

maximum height and increasing their overall length). It is characteristic that for both channel diameters, the period of the capillary ridge formation, coincides with the period of a complete pressure oscillation at the inlet (i.e. every 2 ms for cases A1 and B1, every 1.33 ms for cases A2 and B2 and every 1 ms for cases A3 and B3). It is also evident that, the increase in the pressure oscillation frequency at the inlet of the considered micro-channel in each case, is accompanied by a corresponding reduction in the maximum height of the periodically generated capillary ridge. Some interesting inertial phenomena are also evident, that result in liquid jets penetrating at the rear end of the bubbles leading to the encapsulation of small liquid droplets and fingers within the elongated vapour bubbles and/or in the detachment of small satellite bubbles from its leading and/or its trailing edges. The proposed inertia generated interfacial phenomena are more enhanced in the 1.0 mm internal diameter channel, that in most cases lead to the complete break-up of elongated vapour bubbles into 2 or more parts. Similar, trends were also observed for the rest of the working fluids, however the visualisation results from these working fluids are not presented here due to space limitations.

In order to quantify the effect of the flow oscillation frequency, in the evaporation of the liquid film between the elongating vapour slugs and the heated wall of the channel, the vapour slug volume increase with time is plotted for each of the considered working fluids in Fig. 6.

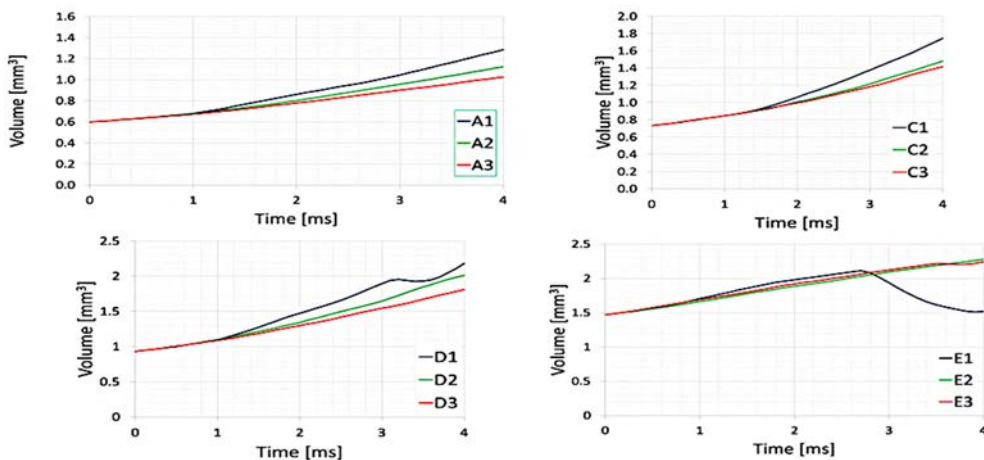


Figure 6: Vapour slug volume with respect to time for R245fa (A1, A2, A3), FC72 (C1, C2 and C3), ethanol (D1, D2 and D3) and water (E1, E2 and E3) for different oscillation frequencies.

As it can be observed, for all four simulated working fluids, the increase in flow oscillation frequency causes a significant decrease in the liquid film evaporation. It seems however that as the frequency increases further that the proposed effect becomes progressively less intense (e.g. C2 to C3 in comparison to C1 to C2 transition). In the case of ethanol and water and for flow oscillation frequency of 500 Hz (D1 and E1), just after around $t = 3$ ms in both cases, a decrease in the vapour volume is observed. This can be attributed to the significant amount of liquid that has been encapsulated in the form of liquid droplets, jets and fingers, within the elongating vapour slugs in these cases.

3.3 Effect of flow oscillation amplitude

The spatial and temporal evolution of the considered vapour slugs in the case of R245fa, under different pressure oscillation amplitudes at the inlet of the considered micro-channel, are depicted in Figs 7 and 8 for the $D_i = 0.5$ mm and $D_i = 1.0$ mm channels respectively. Fig. 7 depicts the numerical simulation results for cases A4–A7, while Fig. 8 illustrates the corresponding results for cases B4–B7. In more detail, in both cases the frequency of the pressure oscillation is kept constant to 500 Hz and the amplitude is increased progressively taking the values of 50, 75, 100, 200 and 300 kPa. In this case it is evident that, the increase in the pressure oscillation amplitude at the inlet of the considered micro-channel in each case, is accompanied by a corresponding increase in the maximum height of the periodically generated capillary ridge. In some cases, the height of the formed capillary ridge reaches the channel radius causing the bubble to break up into 2 parts at this point (see for example highlighted red square number 5 in Fig. 7 and squares number 3, 4 and 5 in Fig. 8). Also, here inertial phenomena are also evident, that result in liquid jets penetrating at the rear end of the bubbles leading to the encapsulation of small liquid droplets jets and fingers within the elongated vapour bubbles and/or in the detachment of small satellite bubbles from its leading and/or its trailing edges.

The proposed inertia generated interfacial phenomena are more enhanced in the 1.0 mm internal diameter channel, that in most cases lead to the complete break-up of elongated vapour bubbles into two or more parts. Moreover, these become more intense as the amplitude of the flow oscillation increases. Similar, trends were also observed for the rest of the working fluids, however the visualisation results from these working fluids are not

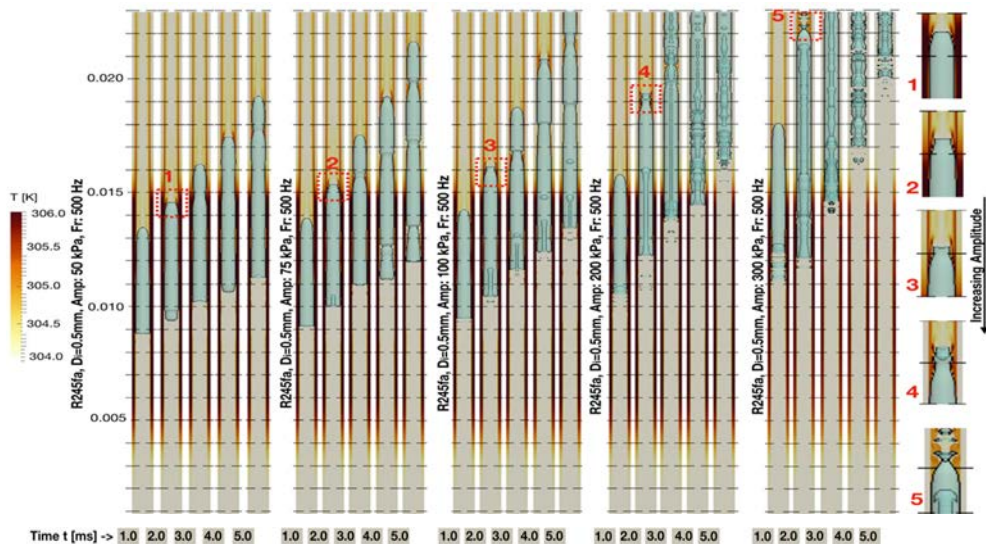


Figure 7: Spatial and temporal evolution of the considered vapour slugs in the case of R245fa, under different pressure oscillation amplitudes at the inlet of the considered micro-channel ($D_i = 0.5$ mm). Cases A4, A5, A1, A6 and A7 (left to right), from Table 1. The red numbered squares mark the initiation of the first capillary ridge in each case. A zoomed version of these instances for each case is also provided.

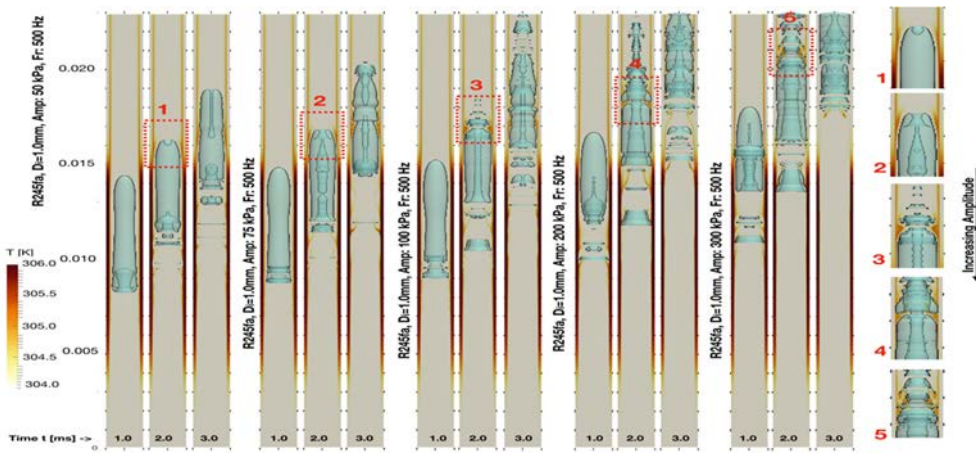


Figure 8: Spatial and temporal evolution of the considered vapour slugs in the case of R245fa, under different pressure oscillation amplitudes at the inlet of the considered micro-channel ($D_i = 1.0$ mm). Cases B4, B5, B1, B6 and B7 (left to right), from Table 1. The red numbered squares mark the initiation of the first capillary ridge in each case. A zoomed version of these instances for each case is also provided.

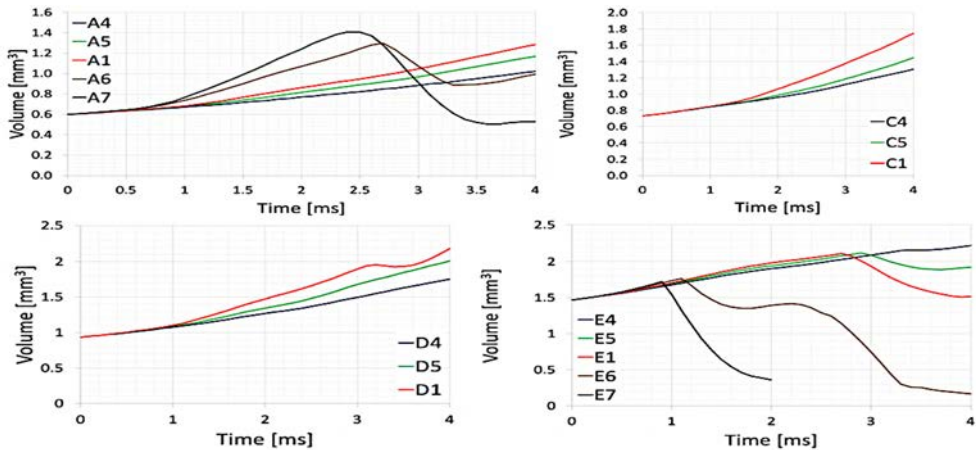


Figure 9: Vapour slug volume with respect to time for R245fa (A4, A5, A6 and A7), FC72 (C4, C5 and C1), ethanol (D4, D5 and D1) and water (E4, E5, E1, E6 and E7) for different oscillation amplitudes.

presented here due to space limitations. In order to quantify the effect of the flow oscillation amplitude, in the evaporation of the liquid film between the elongating vapour slugs and the heated wall of the channel, the vapour slug volume increase with time is plotted for each of the considered working fluids in Fig. 9.

As it can be observed, for all four simulated working fluids, the increase in flow oscillation amplitude, for the initial stages of the bubble growth, causes a corresponding increase in the liquid film evaporation. It seems in most cases that as the amplitude of the oscillation increases further that the proposed effect becomes progressively more intense (e.g. C4 to C5 in comparison to C5 to C1 transition). In all working fluid cases apart from FC72 and for specific oscillation amplitudes, at a certain in each case time instance, which varies in relation to both the oscillation amplitude and the working fluid, a reduction in the vapour volume with respect to time is observed. This can be attributed to the significant amount of liquid that has been encapsulated in the form of liquid droplets, jets and fingers, within the elongating vapour slugs in all these cases, and also to the fact that in some cases the bubble has already exited the channel outlet.

4 CONCLUSIONS

In the present paper, a previously validated and optimized, enhanced, VOF-based numerical modelling framework is applied in order to identify and quantify the effects of global flow oscillation frequency and amplitude on the liquid film evaporation and instabilities formation, around isolated, elongated vapour slugs, within heated micro-channels, in saturated flow boiling conditions. Four different working fluids are considered. From the post-processing and analysis of the results it is obvious that after the application of the induced flow oscillation, capillary ridges are periodically formed in the liquid film between the vapour slug and the heated wall of the channel, in the vicinity of the trailing edge of the elongating bubbles, as they preferentially move towards the outlet. It is shown that the period of formation coincides with the period of the induced flow oscillations for all working fluids tested and that the increase in the flow oscillation frequency, is accompanied by a reduction in the maximum height of the periodically generated capillary ridges, while the increase in the flow oscillation amplitude, causes a corresponding increase in their maximum height that for high oscillation amplitudes can eventually lead to the bubble break-up into two or more parts. Finally, it is found that the liquid film evaporation rate is significantly enhanced by the corresponding increase of the flow oscillation amplitude, while it degrades by the increase of the flow oscillation frequency. For future investigations the content of the present paper can be further extended by performing similar parametric numerical investigations for longer channels and for different applied heat fluxes in order to examine the effect of flow oscillation characteristics in cases of different initial bubble lengths.

ACKNOWLEDGEMENTS

The authors would like to acknowledge the UK's Engineering and Physical Science Research Council support, through the grant EP/P013112/1 as well as the financial support from ESA MAP Projects INWIP and ENCOM 3.

REFERENCES

- [1] Magnini, M., Pulvirenti, B. & Thome, J.R., Numerical investigation of hydrodynamics and heat transfer of elongated bubbles during flow boiling in a microchannel. *Int. J. Heat Mass Transf.*, **59**, pp. 451–471, 2013.
- [2] Szczukiewicz, S., Magnini, M. & Thome, J.R., Proposed models, ongoing experiments, and latest numerical simulations of microchannel two-phase flow boiling. *Int. J. Multiph. Flow*, **59**, pp. 84–101, 2014.
- [3] Lee, J. & Kim, S.J., Effect of channel geometry on the operating limit of micro pulsating heat pipes. *Int. J. Heat Mass Transf.*, **107**, pp. 204–212, 2017.



- [4] Mangini, D., Mameli, M., Georgoulas, A., Araneo, L., Filippeschi, S. & Marengo, M., A pulsating heat pipe for space applications: Ground and microgravity experiments. *Int. J. Therm. Sci.*, **95**, 2015.
- [5] Brackbill, J., Kothe, D. & Zemach, C., A continuum method for modeling surface tension. *J. Comput. Phys.*, **100**(2), pp. 335–354, 1992.
- [6] Hoang, D.A., van Steijn, V., Portela, L.M., Kreutzer, M.T. & Kleijn, C.R., Benchmark numerical simulations of segmented two-phase flows in microchannels using the Volume of Fluid method. *Comput. Fluids*, **86**, pp. 28–36, 2013.
- [7] Deshpande, S.S., Anumolu, L. & Trujillo, M.F., Evaluating the performance of the two-phase flow solver interFoam. *Comput. Sci. Discov.*, **5**(1), p. 14016, 2012.
- [8] Georgoulas, A., Koukouvinis, P., Gavaises, M. & Marengo, M., Numerical investigation of quasi-static bubble growth and detachment from submerged orifices in isothermal liquid pools: The effect of varying fluid properties and gravity levels. *Int. J. Multiph. Flow*, **74**, pp. 59–78, 2015.
- [9] Hardt, S. & Wondra, F., Evaporation model for interfacial flows based on a continuum-field representation of the source terms. *J. Comput. Phys.*, **227**(11), pp. 5871–5895, 2008.
- [10] Georgoulas, A., Andredaki, M. & Marengo, M., An enhanced VOF method coupled with heat transfer and phase change to characterise bubble detachment in saturated pool boiling. *Energies*, **10**(3), 2017.
- [11] Teodori, E., Pontes, P., Moita, A., Georgoulas, A., Marengo, M. & Moreira, A., Sensible heat transfer during droplet cooling: Experimental and numerical analysis. *Energies*, **10**(6), 2017.
- [12] Andredaki, M., Georgoulas, A., Miché, N. & Marengo, M., Break-up mechanisms and conditions for vapour slugs within mini-channels. *15th UK Heat Transfer Conference, UKHTC2017*, Brunel University, London, 4–5 September, 2017.

